

Effect of Sulfur on Corrosion Behavior of Pulse Plated Nanocrystalline Ni

*S.H. Kim, K. T. Aust & U. Erb, Dept. of Materials Science & Engineering, University of Toronto, Toronto, Canada; G.Ogundele, Kinectrics Inc., Toronto, Canada;
F. Gonzalez, Integran Technologies Inc., Toronto, Canada*

The effect of sulfur on the corrosion behavior of nanocrystalline Ni produced by pulse plating has been studied in solutions of varying pH. Potentiodynamic polarization in conjunction with energy dispersive X-ray spectroscopy was used to investigate the role of sulfur on the passivation behavior of nanocrystalline Ni. Cross-sectional examination by scanning electron microscopy demonstrated that the unique structure of the nanocrystalline state promoted uniform dissolution that would minimize the risk of catastrophic failure by localized attack.

For more information, contact:

S. Kim c/o Prof. U. Erb
Dept. of Materials Science and Eng.
University of Toronto
Toronto, Ontario
Canada, M5S 3E4

1.0 Introduction

Intergranular corrosion is a localized form of material degradation which can lead to significant mass loss, rapid deterioration of structural integrity and, as a result, unpredictable catastrophic failure in many conventional and advanced materials. In the past, there have been numerous attempts to alleviate the intergranular corrosion by controlling some of the factors that lead to this detrimental form of corrosion including impurity segregation¹, electrochemical environment², grain boundary character distribution³, second phase particles⁴ and residual stress⁵.

In recent years, the grain size of polycrystalline materials has been found to have a significant influence on the grain boundary corrosion, particularly in nanocrystalline Ni and Ni alloys⁶⁻⁸. Contrary to earlier expectations, it has been shown that reducing the grain size in these materials below 100 nm can effectively eliminate intergranular corrosion by delocalizing the attack over the entire surface⁶⁻⁸. This is probably a result of increasing the anode (interface) to cathode (grain interior) area ratio by several orders of magnitude⁷.

In addition, for many metals, impurities are known to be detrimental in polycrystalline materials because of their segregation to grain boundaries during thermomechanical treatments and subsequent initiation of intergranular corrosion⁹. It was proposed¹⁰ that nano-processing provides an opportunity to improve the resistance to solute segregation by a solute dilution effect. It has been previously shown that the intercrystalline volume fraction (i.e., the total fraction of atoms associated with grain boundaries and triple junctions) which is less than 0.03% for conventional polycrystalline material with 10 μ m grain size, increases rapidly with decreasing grain size (d) below 100 nm, following a 1/d³ relationship¹¹. Using a typical grain boundary thickness of 1 nm, this volume fraction approaches 50% at a grain size of 5 nm. Furthermore, assuming complete segregation of all bulk impurities to grain boundaries and triple junctions, the maximum attainable grain boundary impurity segregation can be computed¹⁰. For example, such analysis has shown that, for a total bulk impurity content of 100 ppm, the grain boundary concentration at maximum segregation reaches a value of about 30% in a conventional polycrystalline material with 10 μ m grain size. In contrast, by reducing the grain size to 10 nm, the maximum solute concentration would only be about 0.03%. In other words, in addition to providing more beneficial anode/cathode ratios based on geometrical considerations, nanocrystalline materials (at the same level of impurities) contain significantly “cleaner” grain boundaries than materials with grain sizes in the micrometer range, which should ultimately result in reduced susceptibility to intergranular corrosion.

Recent advances in the cost-effective manufacturing of fully dense nanocrystalline metals and alloys via the pulsed current electrodeposition process¹² have resulted in numerous emerging industrial applications of these materials either as thin and thick coatings or free-standing structures¹³. In particular, the mechanical, physical and chemical properties of nanocrystalline Ni have been studied extensively¹⁴. Sulfur is one specific impurity of interest in nanocrystalline Ni because this material is often produced from plating baths containing sulfur bearing additives, e.g. saccharin, from which sulfur in concentrations of several hundred ppm can be codeposited with nanocrystalline Ni¹⁵. A study of the influence of sulfur on the corrosion behavior of nanocrystalline Ni is therefore, not only of direct interest for industrial applications, but also provides an excellent system for the study of the impurity dilution effect.

2.0 Experimental Procedure

In this study, polycrystalline Ni200, nanocrystalline Ni and annealed nanocrystalline Ni samples, all in the shape of cylinders having dimensions of 1.25cm in diameter and 1cm in length, were used. The polycrystalline Ni200 material with an average grain size of \sim 50 μ m was purchased from Alfa Aesar.

Nanocrystalline Ni samples of $\sim 650\mu\text{m}$ in thickness were produced by electrodeposition from a saccharin-containing Watt's bath on the outer diameter (OD) of carbon steel rods using a procedure described elsewhere¹². The average grain size was found to be $\sim 30\text{nm}$ as determined by transmission electron microscopy. Infrared adsorption analysis revealed that the nanocrystalline Ni contained ~ 1080 ppm of sulfur. Some of the as-deposited nanocrystalline Ni samples were annealed at $\sim 950^\circ\text{C}$ for 15 min. in argon in order to obtain polycrystalline Ni through grain growth with the same overall sulfur content as nanocrystalline Ni. In addition to extensive grain growth, this annealing treatment also resulted in sulfur segregation to grain boundaries and subsequent formation of grain boundary precipitates (various Ni_xS_y as per equilibrium phase diagram¹⁶). The OD surfaces of all samples were ground to grit size #600 SiC paper within 1 hour of electrochemical testing, followed by ultrasonic cleaning in acetone. The potentiodynamic polarization experiments were performed using a 1286 Electrochemical Interface manufactured by Solartron Instruments and a glass polarization cell similar to the one described in ASTM-G5.

Two electrolytes were used in this study. The first solution contained 0.25M sodium sulfate (Na_2SO_4) prepared by using reagent chemicals dissolved in deionized water having electrical resistivity of $1\text{M}\Omega$. The pH of the solution was ~ 6.5 . The second electrolyte was a 1 vol% ammonium hydroxide (NH_4OH) solution of pH ~ 11.5 at room temperature. An assessment of the corrosion behavior of Ni in the latter solution is of considerable technological importance. For example, NH_4OH is currently used to control the pH in the secondary side of steam generators in CANDU nuclear power generating stations where 1 mm thick nanocrystalline nickel alloys were recently applied for structural in-situ repair of degraded steam generator tubing¹⁷.

3.0 Results and Discussion

3.1 Corrosion behavior in Na_2SO_4 solution (pH = 6.5)

Figure 1 shows the anodic polarization behavior of polycrystalline Ni200, as-plated nanocrystalline and annealed nanocrystalline Ni in deaerated 0.25M Na_2SO_4 (pH = 6.5). The polycrystalline Ni200 displayed a distinct passive region between the voltages of 0 and $0.5V_{\text{SCE}}$ which is consistent with previous studies conducted in Na_2SO_4 solutions¹⁸⁻²⁰. In the case of as-plated nanocrystalline Ni, the passive region in the potentiodynamic curve is virtually eliminated. It was earlier demonstrated in a study by Kim et al.²¹, that the reduced passivity for as-plated nanocrystalline Ni was due to the high sulfur content (in the current study: ~ 1080 ppm) introduced during electrodeposition.

Also included in Figure 1 is the potentiodynamic polarization curve for the nanocrystalline Ni annealed at 950°C for 15 min. The annealing resulted in a polycrystalline Ni with an average grain size of about $100\mu\text{m}$. The polarization curve of the annealed nanocrystalline Ni was found to be almost identical to that of as-plated nanocrystalline Ni, indicating that sulfur has the same effect in both materials: it reduces the passivity of Ni, regardless of grain size.

Despite the similar potentiodynamic polarization curves observed for as-plated nanocrystalline Ni and annealed nanocrystalline Ni shown in Figure 1, a considerable difference in their corrosion morphologies was noted in the scanning electron microscope (SEM) as shown in Figure 2. In the case of as-plated nanocrystalline Ni, the surface is covered with a high density of shallow pits which were most likely formed as a result of sulfur blocking the sites for adsorption of hydroxyl ions, known as the precursor in the formation of a passive layer²², preventing the formation of a stable passive film. According to a 3-D atom probe study by Warren et al.²³, sulfur impurities (1000 ppm) in electrodeposited nanocrystalline Ni are uniformly dispersed throughout the structure. Therefore, it is not surprising that the pits formed on the

surface of as-plated nanocrystalline Ni (Figure 2a) are evenly distributed over the entire surface. However, in the case of annealed nanocrystalline Ni, extensive localized attack was observed along grain boundaries where enrichment of sulfur would be expected after the heat treatment (Figure 2b). In fact, in a combined scanning transmission electron microscopy/energy-dispersive X-ray spectroscopy study, Klement et al.²⁴ found that there was already significant enrichment of sulfur at the grain boundaries after annealing nanocrystalline Ni containing 1580ppm sulfur for 30 min. at 220°C. Kim and Oriani¹⁹ also observed that polycrystalline Ni, when doped with sulfur by exposure to SO₂ at 1 atm and 800°C for 10 min., did not passivate in the same environment (0.25M Na₂SO₄), due to extensive intergranular corrosion caused by second phase particles, nickel sulfides, which formed mainly along grain boundaries.

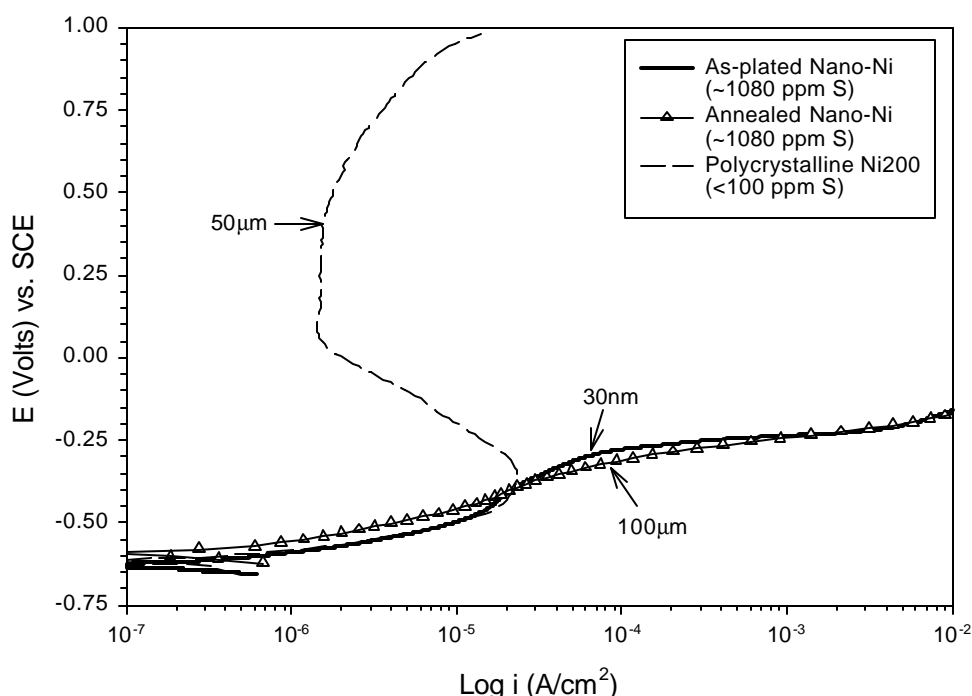


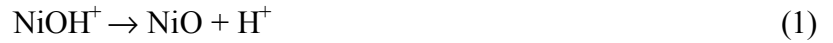
Figure 1 Potentiodynamic polarization curves obtained in deaerated 0.25M Na₂SO₄ at pH = 6.5 (indicted with arrows are the average grain sizes of each material used, scan rate = 0.2 mV/sec).

When cross-sections of both as-plated and annealed nanocrystalline Ni were examined in the SEM, a more drastic difference was noted as shown in Figure 3. For the annealed nanocrystalline Ni, the localized grain boundary corrosion penetrated as deep as 130μm into the deposit, which resulted in “grain dropping” in some areas (Figure 3a). However, in the case of nanocrystalline Ni, the uniformly distributed pits on the surface as shown in Figure 2(a) were very shallow, usually less than 2μm in depth (Figure 3b). A similar delocalized corrosion attack in nanocrystalline Ni has been previously shown in other environments including 2N H₂SO₄ solution (pH = 0)⁶ and 30 wt% KOH solution (pH ≈ 14.8)⁸.

3.2 Corrosion behavior in NH₄OH solution (pH = 11.5)

Figure 4 shows the potentiodynamic polarization curves for polycrystalline Ni200, as-plated nanocrystalline Ni and annealed nanocrystalline Ni in deaerated 1 vol% NH₄OH solution (pH=11.5). The as-plated nanocrystalline Ni, unlike in 0.25M Na₂SO₄ solution at pH=6.5 (Figure 1), shows nearly identical active, passive and transpassive behavior as observed for conventional polycrystalline Ni200.

This is consistent with results reported in an earlier study by Kim et al.²¹ in which, in Na₂SO₄ solution with 50 ppm NaOH (pH ~10.9), the polarization curves for polycrystalline Ni200 and as-plated, sulfur-containing nanocrystalline Ni were found to be the same, both showing well-defined passive regions. This can be explained as follows. At high pH, (i.e. lower H⁺ concentration), a lower concentration of NiOH⁺ is required for the passivation reaction (1) to occur since the saturation concentration, [NiOH⁺]_s, follows a solubility product (K_{sp}) as shown in equation (2)²⁵.



$$K_{\text{sp}} = [\text{NiOH}^+]_s / [\text{H}^+] \quad (2)$$

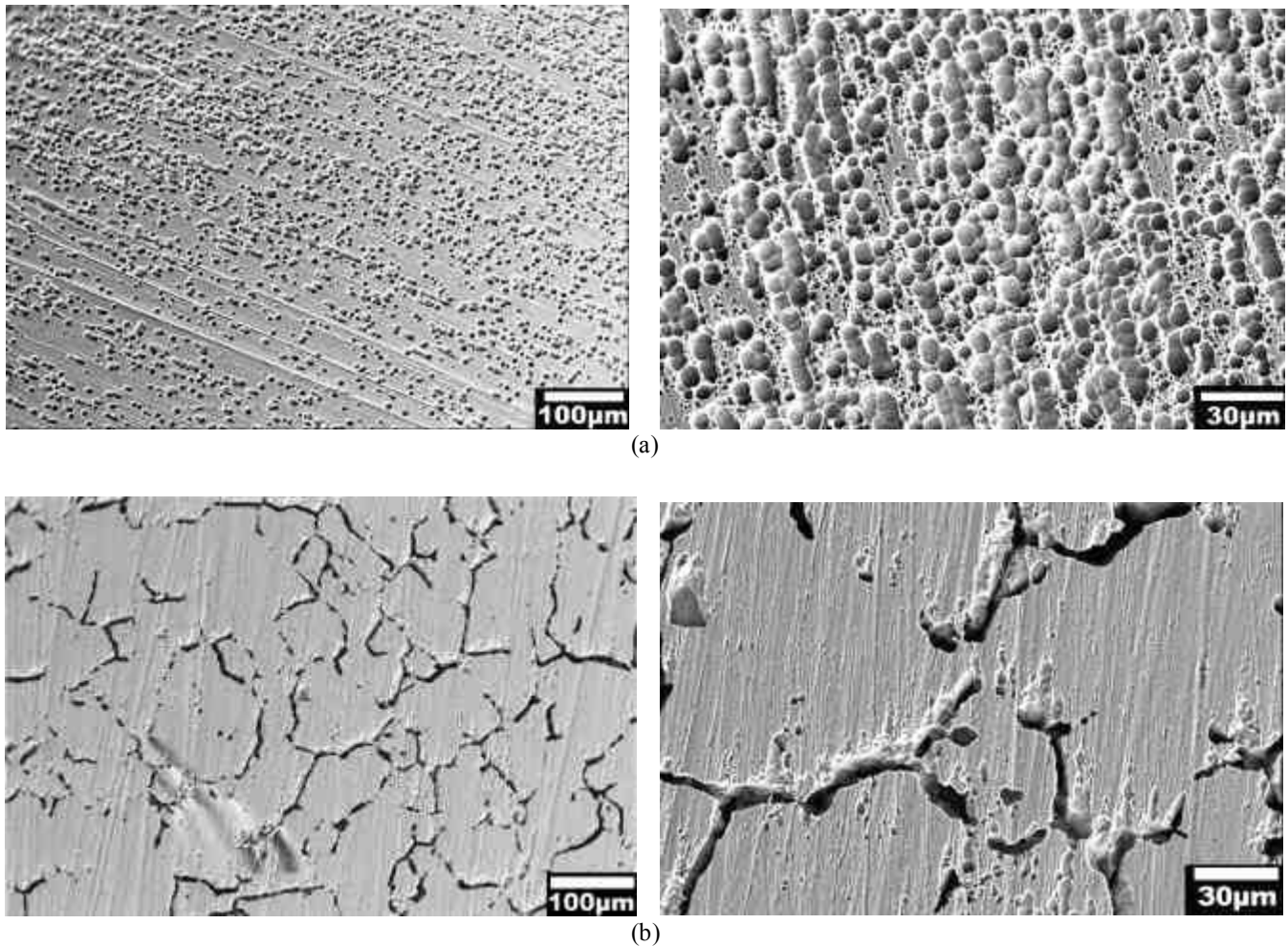
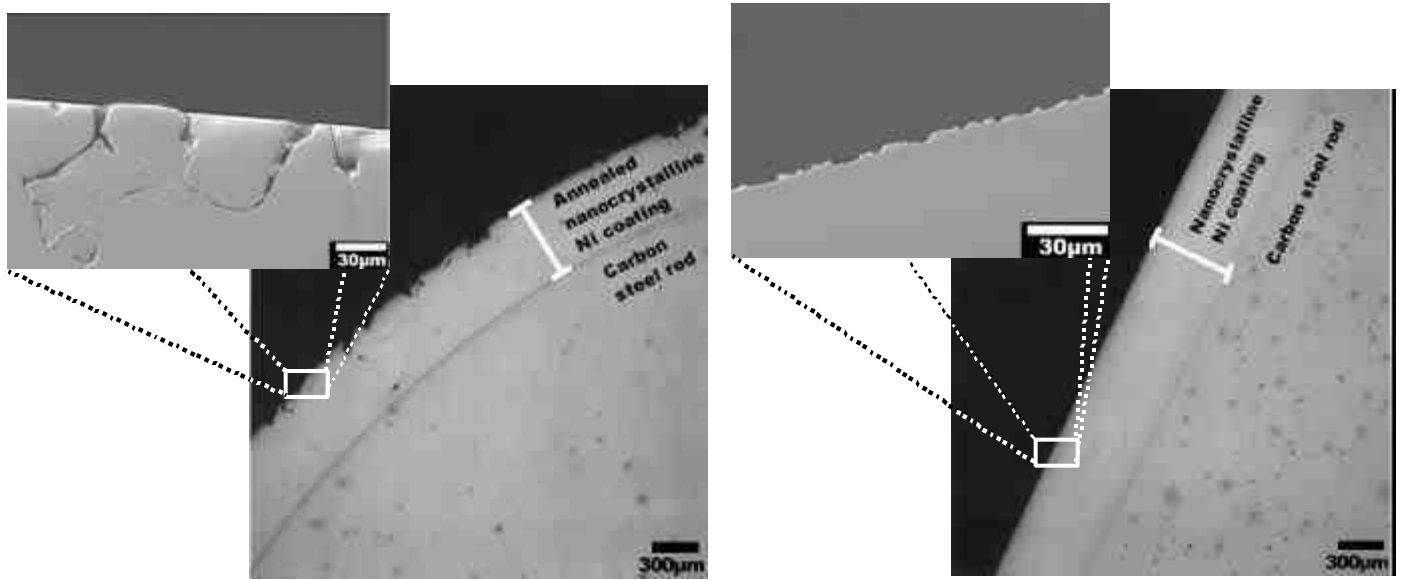


Figure 2 SEM images at two different magnifications showing the corrosion morphologies following potentiodynamic testing in deaerated 0.25M Na₂SO₄ of (a) as-plated nanocrystalline Ni, (b) annealed nanocrystalline Ni (950°C for 15min.).



(a)

(b)

Figure 3 Cross-sectional examination of corroded samples of (a) annealed nanocrystalline Ni and (b) as-plated nanocrystalline Ni.

In addition, another significant parameter in passivation is the Flade potential²⁶. The Flade potential, E_F , is the potential at which the transition from active to passive occurs. It was previously found that E_F of many metals such as iron, chromium, Cr-Fe alloys and nickel generally follows a linear relationship with pH in the following form²⁷:

$$E_F = E_F^\circ - 0.059\text{pH} \quad (3)$$

where E_F° is the Flade potential at pH = 0. Therefore, reduced metal dissolution combined with a more negative potential at which a passive layer forms at higher pH enable nanocrystalline Ni to form a passive film prior to accumulating on the surface a critical amount of sulfur²², above which a non-protective sulphide film forms.

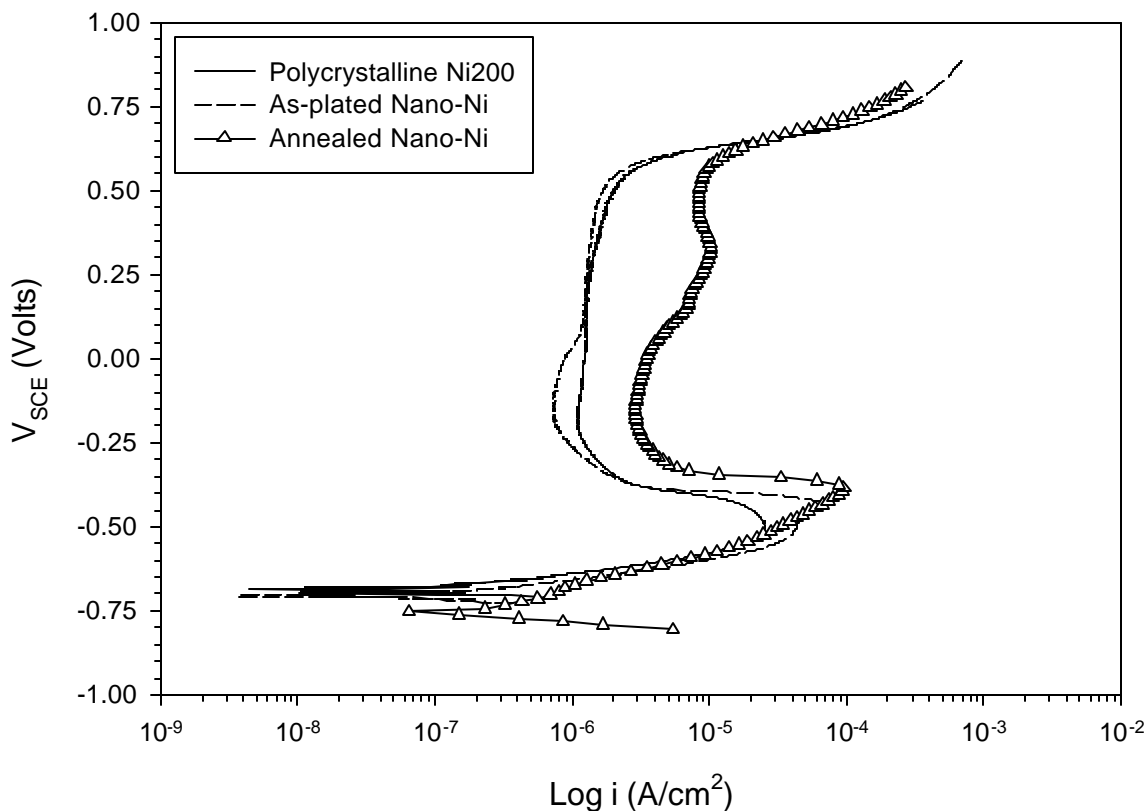


Figure 4 Potentiodynamic polarization curves obtained in deaerated 1 vol% NH_4OH ($\text{pH} = 11.5$, scan rate = 0.2 mV/sec).

An interesting observation in Figure 4 is that, despite showing qualitatively the same active-passive-transpassive behaviour, the annealed nanocrystalline Ni exhibits a higher passive current density. For example, at a potential of $0.3V_{\text{SCE}}$, the passive current densities for Ni200 and as-plated nanocrystalline Ni are $\sim 1\mu\text{A}/\text{cm}^2$ whereas the passive current density for annealed nanocrystalline Ni is $\sim 10\mu\text{A}/\text{cm}^2$. In an attempt to understand this phenomenon, some samples of both as-plated and annealed nanocrystalline Ni were potentiodynamically polarized up to a potential of $0V_{\text{SCE}}$ in deaerated 1 vol% NH_4OH at which both exhibit passivation and then immediately removed from the corrosion cell for surface examination in the SEM. Whereas the surface of as-plated nanocrystalline Ni showed nearly no resolvable damage (except the scratches remnant from grinding, Figure 5a), the surface of the annealed nanocrystalline Ni showed already considerable preferential attack (Figure 5b), especially along triple junctions and grain boundaries (Figure 6). This localized attack on the annealed nanocrystalline Ni is due to the nickel sulfide precipitates that form during grain growth²⁸. Although

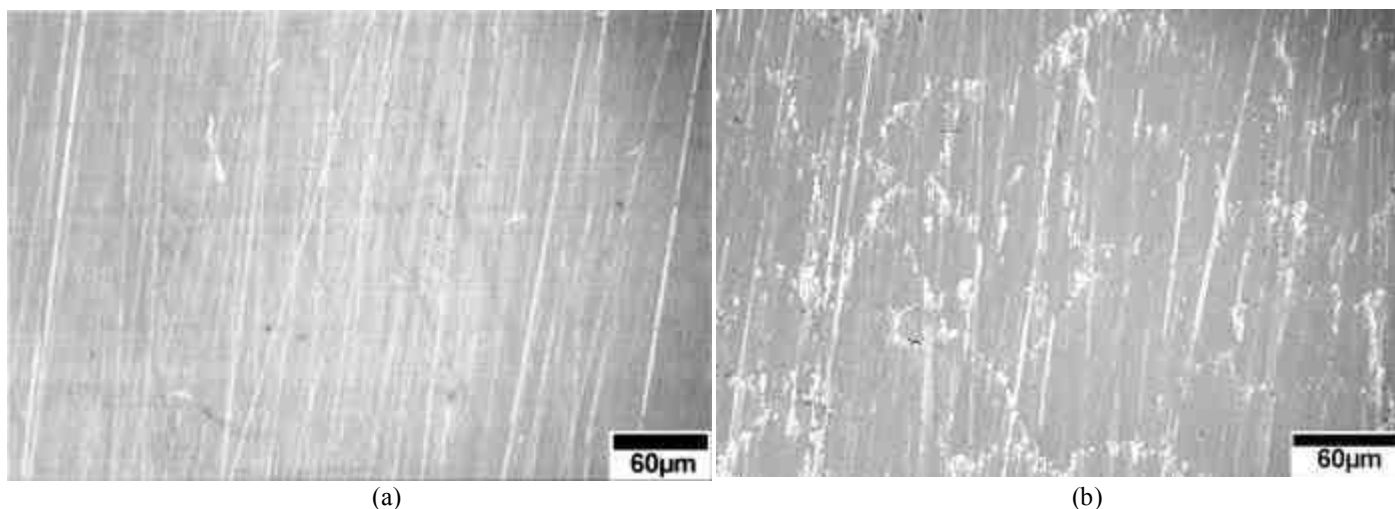


Figure 5 SEM images showing the surfaces of (a) as-plated nanocrystalline Ni and (b) annealed nanocrystalline Ni after potentiodynamic polarization testing up to $0 V_{SCE}$ in deaerated 1 vol% NH_4OH solution.

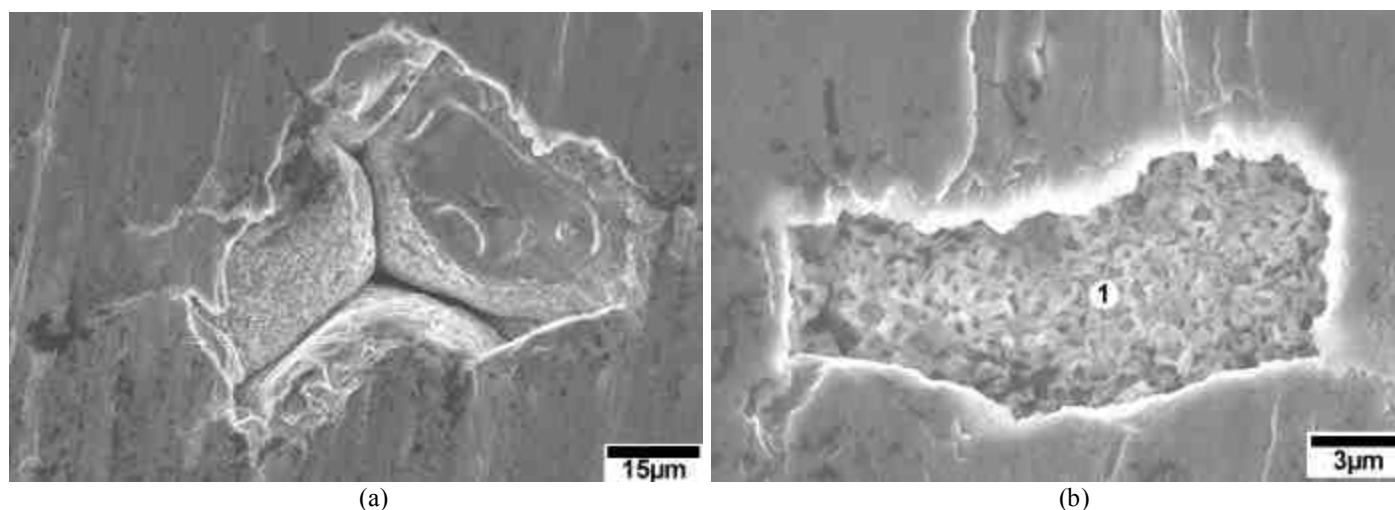


Figure 6 High magnification SEM images of the annealed nanocrystalline Ni (Figure 5(b)) showing preferential dissolution at (a) a triple junction and (b) a grain boundary.

most of the surface-near nickel sulfide precipitates have been dissolved during polarization up to the potential of $0V_{SCE}$, many pits still show some sulfur residues as shown by the EDS spectrum (Figure 7) taken at the bottom of the grain boundary pit shown in Figure 6b. Nickel sulfide precipitates were also reported to initiate pitting in annealed Ni200 with much lower sulfur concentrations, particularly in NaCl environments²⁹⁻³⁰. Datta and Landolt²⁹, after observing preferential pit formation on sulfides during high rate dissolution of Ni200 in 5M NaCl, suggested the following mechanisms for pit formation. First, assuming the precipitates to be poor electrical conductors, the current density between inclusion and metal is locally increased resulting in non-uniform current distribution which, in turn, could lead to preferential dissolution around the precipitates. Second, voids between the inclusions and the metal could form during cooling due to the difference in the thermal expansion coefficient. These voids could then act as nucleation sites for preferential pitting. Finally, the precipitates themselves may undergo chemical or electrochemical dissolution and release sulfur ions that according to Oudar and Marcus²², can act as catalyst for anodic dissolution of Ni. Therefore, it is likely that the large amount of sulfur shifted the

passive current density to a higher value when nickel sulfide precipitates are formed during the annealing of nanocrystalline Ni.

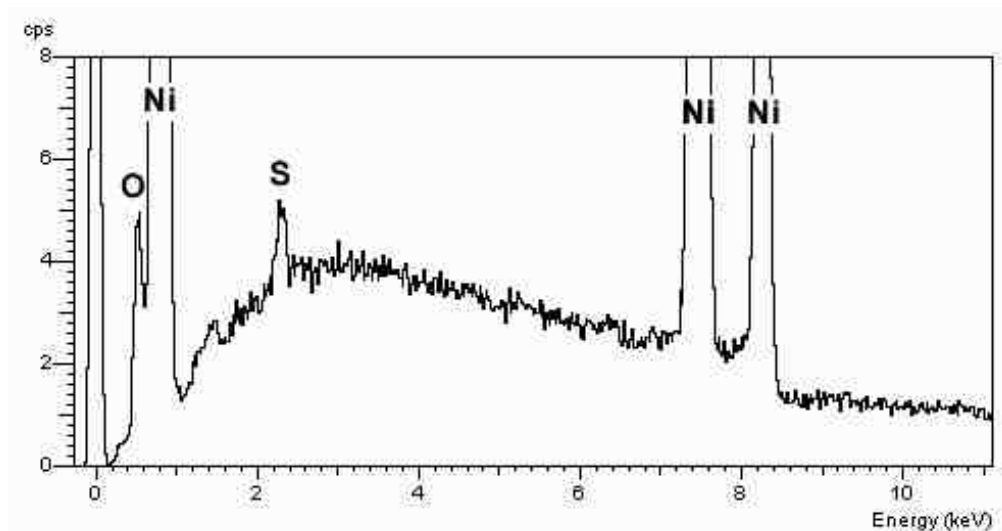


Figure 7 EDS analysis of region 1 shown in Figure 6 (b).

4.0 Summary

In 0.25M Na₂SO₄ solution (pH = 6.5), the presence of 1080 ppm sulfur reduced the passivity of both as-plated and annealed nanocrystalline Ni. However, even at such a high concentration of sulfur, as-plated nanocrystalline Ni is highly resistant to localized corrosion while the annealed polycrystalline counterpart with the same sulfur-content resulted in highly localized attack with grain dropping. At higher pH (pH = 11.5, 1 vol% NH₄OH solution), both as-plated and annealed nanocrystalline Ni with 1080 ppm sulfur displayed passive behavior comparable to that of conventional polycrystalline Ni200. However, the passive current density for the annealed nanocrystalline Ni was approximately 1 order of magnitude higher and localized grain boundary/triple junction attack on Ni sulfide precipitates was observed. The results of this study support the earlier hypothesis that solute dilution by nano-processing can be used as an effective metallurgical tool to improve the overall intergranular degradation resistance of Ni, in particular, when high levels of sulfur impurities are present in the material. The delocalised corrosion observed for nanocrystalline Ni is of tremendous technological importance. Regardless of whether or not the material passivates, a highly uniform metal dissolution is desirable because for lifetime assessment considerations, the total material loss can be designed for as long as the corrosion rate is known. For the case of polycrystalline materials with localized grain boundary attack, this is not possible and catastrophic failures must be anticipated.

Acknowledgements

Financial support by the Natural Sciences and Engineering Research Council of Canada (NSERC), Ontario Power Generation, Kinectrics and Integran Technologies is gratefully acknowledged. Fruitful discussions with Prof. D. Kirk are also acknowledged.

References

1. G. Palumbo and K. T. Aust, *Acta Met. et Mat.*, **38**, 2343 (1990).
2. K. Osozawa, K. Bohenkamp and H. J. Engell, *Corros. Sci.*, **6**, 421 (1966).
3. P. Lin, G. Palumbo, U. Erb and K. T. Aust, *Scripta Met. et. Mat.*, **33**, 1387 (1995).
4. A. Joshi and D. F. Stein, *Corrosion*, **28**, 321 (1972).
5. S. Haruyama, *Materials Performance*, No 3, 14 (1982).
6. R. Rofagha, R. Langer, A.M. El-Sherik, U. Erb, G. Palumbo and K.T. Aust, *Scripta Met. et. Mat.*, **25**, 2867 (1991).
7. S. Wang, *Electrochemical Properties of Nanocrystalline Ni and Ni-Mo Alloys*, Ph.D. Thesis, Queen's University, Kingston, Ontario, Canada, 1997.
8. S. Wang, R. Rofagha, P. R. Roberge and U. Erb, *Electrochem. Soc. Proc.* **95-8**, 244 (1995).
9. U. R. Evans, *The Corrosion and Oxidation of Metals: Scientific Principles and Practical Applications*, Edward Arnold Ltd., London, 1960; p.660.
10. G. Palumbo and U. Erb, *MRS Bulletin*, **24**, No. 11, 27 (1999).
11. G. Palumbo, S. J. Thorpe and K. T. Aust, *Scripta Met. et. Mat.*, **24**, 1347 (1990).
12. U. Erb and A. M. El-Sherik, U.S. Patent No. 5,352,266 (October 4, 1994).
13. A. Roberson, U. Erb and G. Palumbo, *Nanostr. Mat.*, **12**, 1035 (1999).
14. U. Erb, K. T. Aust, G. Palumbo, J. McCrea and F. Gonzalez in Processing and Fabrication of Advanced Materials IX, T.S. Srivatsan et al. (eds), ASM International, Materials Park, OH, 253 (2001).
15. A.M. El-Sherik and U. Erb, *J. Mater. Sci.*, **30**, 5743 (1995).
16. ASM Metals Handbook, Volume 3 Alloy Phase Diagrams, H. Baker (ed.), ASM Materials Park, Ohio (1992).
17. F. Gonzalez, A. M. Brennenstuhl, G. Palumbo, U. Erb and P. C. Lichtenberger, *Mater. Sci. Forum*, **225-227**, 831 (1996).
18. B. MacDougall and M. Cohen, *J. Electrochem. Soc.*, **123**, 191 (1974).
19. Y. J. Kim and R. A. Oriani, *Corrosion*, **44**, 360 (1988).
20. R. E. Hummel, R. J. Smith and E. D. Verink JR, *Corros. Sci.* **27**, 803 (1987).
21. S. Kim, F. Gonzalez, G. Panagiotopoulos, G. Palumbo, U. Erb and K. T. Aust, American Electroplaters and Surface Finishers Society, *AESF SUR/FIN*[®], Nashville, AESF, Orlando, Florida, CD-Rom, Section D (2001).
22. J. Oudar and P. Marcus, *Appl. Surf. Sci.*, **3**, 359 (1979).
23. P.J. Warren, M. Thuvander, M. Abraham, H. Lane, A. Cerezo and G.D.W. Smith, *Mater. Sci. Forum*, **343-346**, 701 (2000).
24. U. Klement, U. Erb, A.M. El-Sherik, K.T. Aust, *Mater. Sci. Eng.* **A203**, 177 (1995).
25. N. Sato and G. Okamoto, *J. Electrochem. Soc.*, **110**, 605 (1963).
26. F. Flade, *Z. Physik. Chem.*, **76**, 513 (1911).
27. U. F. Franck, *Z. Naturforschung.*, **4A**, 378 (1949).
28. A.M. El-Sherik, K. Boylan, U. Erb, G. Palumbo and K. T. Aust, *Mat. Res. Soc. Symp. Proc.*, **238**, 727 (1992).
29. M. Datta and D. Landolt, *J. Electrochem. Soc.*, **129**, 1889 (1982).
30. C.H. Paik and R. C. Alkire, *J. Electrochem. Soc.*, **148**, B276 (2001).